

# How to measure absolute P3HT crystallinity via $^{13}\text{C}$ CPMAS NMR

Ryan C. Nieuwendaal\*

**ABSTRACT:** We outline the details of acquiring quantitative  $^{13}\text{C}$  cross-polarization magic angle spinning (CPMAS) nuclear magnetic resonance on the most ubiquitous polymer for organic electronic applications, poly(3-hexylthiophene) (P3HT), despite other groups' claims that CPMAS of P3HT is strictly nonquantitative. We lay out the optimal experimental conditions for measuring crystallinity in P3HT, which is a parameter that has proven to be critical in the electrical performance of P3HT-containing organic photovoltaics but remains difficult to measure by scattering/diffraction and optical methods despite considerable efforts. Herein, we overview the spectral acquisition conditions of the two P3HT films with different crystallinities (0.47 and 0.55) and point out that because of the chemical similarity of P3HT to other alkyl side chain, highly conjugated main chain polymers, our protocol could straightforwardly be extended to other organic electronic materials. Variable temperature  $^1\text{H}$  NMR results are shown as well, which (i) yield insight into the molecular dynamics of P3HT, (ii) add context for spectral editing techniques as applied to quantifying crystallinity, and (iii) show why  $T_{1\rho}^{\text{H}}$ , the  $^1\text{H}$  spin-lattice relaxation time in the rotating frame, is a more optimal relaxation filter for distinguishing between crystalline and noncrystalline phases of highly conjugated alkyl side-chain polymers than other relaxation times such as the  $^1\text{H}$  spin-spin relaxation time,  $T_2^{\text{H}}$ , and the spin-lattice relaxation time in the toggling frame,  $T_{1xz}^{\text{H}}$ . A 7 ms  $T_{1\rho}^{\text{H}}$  spin lock filter, prior to CPMAS, allows for spectroscopic separation of crystalline and noncrystalline  $^{13}\text{C}$  nuclear magnetic resonance signals. Published 2016. This article is a U.S. Government work and is in the public domain in the USA.

**Keywords:** solid-state NMR;  $^{13}\text{C}$  CPMAS; organic electronics; crystallinity; polymer; P3HT; morphology; paracrystallinity

## Introduction

Despite its ubiquitous use in solving problems related to biology, chemistry, and materials science, solid-state nuclear magnetic resonance (NMR) has had relatively little impact in the field of organic electronics (OE). Indeed, despite the prevalent use of the technique in the physical sciences, the number of recent publications where solid-state NMR was utilized to solve critical problems in, for instance, organic photovoltaics remains quite low.<sup>[1–5]</sup> This remains true even though the technique could be used to potentially solve several critical issues that face this field. For example, degrees of mixing in polymer/small molecule blends, polymer chain dynamics, and polymer structural heterogeneity are all problems that have classically been tackled using solid-state NMR, and all of which are important parameters which affect the efficiencies of organic photovoltaic active layers.

Absolute crystallinity is one measurement that could be of particular use to the OE community, because it has been shown that order is an important parameter governing performance.<sup>[6–9]</sup> However, measuring absolute crystallinity has been particularly difficult via by scattering/diffraction<sup>[10,11]</sup> and by optical methods.<sup>[12,13]</sup> NMR has previously been utilized for measuring crystallinities in semicrystalline polymers and has historically been used in classic polymers such as polyethylene and cellulose, whether by  $^{13}\text{C}$  magic angle spinning (MAS) or via  $^1\text{H}$  relaxation methods.

In this paper, we outline the details of acquiring quantitative  $^{13}\text{C}$  cross-polarization magic angle spinning (CPMAS) NMR spectra of poly(3-hexylthiophene) (P3HT), the 'fruit fly' of semiconducting polymers. CPMAS can offer orders of magnitude of time savings

over single pulse excitation (SPE)  $^{13}\text{C}$  MAS NMR, which is the 'gold standard' for quantitative  $^{13}\text{C}$  NMR spectra, but suffers from low signal-to-noise ratios and long acquisition times. Having a fast, robust, and reliable method of acquiring quantitative  $^{13}\text{C}$  NMR spectra could truly impact the OE field because sample sizes of thin films tend to be small (<5 mg), and absolute crystallinity is a measurement that the OE field needs. While other groups have claimed that the  $^{13}\text{C}$  CPMAS of P3HT is strictly nonquantitative,<sup>[14,15]</sup> herein, we lay out the experimental conditions that one can use for *quantitatively* measuring crystallinity in P3HT to within 4%. Furthermore, we layout the subtleties of the CPMAS conditions and explain perhaps why, because of a relatively narrow range of acceptable acquisition parameters (refer to succeeding texts), CPMAS was previously thought to be strictly nonquantitative. The side-chain dynamics of P3HT, which play a critical role in these CPMAS conditions as well as the  $^1\text{H}$ -based relaxation time spectral editing, are investigated via variable temperature  $^1\text{H}$  NMR. The spatial dynamic

\* Correspondence to: Ryan C. Nieuwendaal, National Institute of Standards and Technology, 100 Bureau Drive, Gaithersburg, MD 20899, USA. E-mail: ryann@nist.gov

This work was carried out by the National Institute of Standards and Technology, an agency of the US government, and by statute is not subject to copyright in the USA. Certain commercial equipment, instruments, materials, services, or companies are identified in this paper in order to specify adequately the experimental procedure. This in no way implies endorsement or recommendation by National Institute of Standards and Technology.

National Institute of Standards and Technology, 100 Bureau Drive, Gaithersburg, MD, 20899, USA

heterogeneity of these side-chain dynamics is explored via a comparison of  $^1\text{H}$  SPE and  $T_{1\rho}^{\text{H}}$  and  $T_{1xz}^{\text{H}}$  relaxation time experiments so that  $^1\text{H}$  spin relaxation editing could be applied to  $^{13}\text{C}$  CPMAS spectra, as was shown in previous works of heterogeneous soft matter.<sup>[16]</sup> The characteristics of the dynamic heterogeneity are important because it is desirable to identify a relaxation time which exhibits differences *only* between the crystal and the noncrystal phases and not between different protons within a phase or monomer. Hence, proper crystal/noncrystal deconvolution requires there to be local relaxation time *averaging* smaller than the crystal (<20 nm) but larger than the monomer unit (>1 nm). Only after the full spectrum is broken up into crystal and noncrystal components (based on these relaxation time differences) can the crystallinity be determined via direct integration.

## Results/discussion

### P3HT samples and crystallization

Two P3HT films were cast using different drying rates, one a 'slow dried' film, which dried from chlorobenzene over 4 to 6 h, and another 'fast dried' film, which was drop-cast from chloroform onto a heated substrate (70 °C) and dried in 3 to 5 s. The two films were previously investigated via differential scanning calorimetry (DSC) and X-ray diffraction for crystallinity characterization; we refer readers to our previous publications for more details.<sup>[17,18]</sup> We recently showed that the absolute crystallinity of P3HT could be quantitatively measured from DSC when accounting for crystal size; this value agrees quite well with the value from  $^{13}\text{C}$  NMR. The melt enthalpy, melting temperature, absolute crystallinity, and crystal sizes, as measured from DSC, are all tabulated in Table 1 (left side). From DSC, the two films exhibit similar crystallinities ( $x_c=0.45$  and 0.62), but because of their disparate crystal sizes, exhibit different melt enthalpies and temperatures.<sup>[18]</sup> The NMR values (Table 1, right side) will be discussed in the succeeding texts.

### Quantitative $^{13}\text{C}$ CPMAS NMR

Because  $^{13}\text{C}$  resonance positions are typically sensitive to local chain packing, the linewidths observed in  $^{13}\text{C}$  spectra are diagnostic of packing uniformity. A CPMAS spectrum of the fast-dried film taken at 2.35 T is given in Fig. 1a, which also displays the assignments. Carbons labeled 1–6 (C1–C6) are the aliphatic carbons; 7–10 are thiophene (C7–C10). Clearly, the spectrum (Fig. 1a) comprises multiple components; the narrower peaks are due to ordered chains and the broader components due to disordered chains as we laid out previously.<sup>[16]</sup> We will discuss the relaxation-based deconvolution (i.e. spectral editing) process in the succeeding texts (Fig. 1b–k) but first discuss the experimental conditions that allow for quantitative  $^{13}\text{C}$  NMR spectra.

**Table 1.** DSC and NMR data of P3HT films of different drying rates

Film	DSC				NMR	
	Enthalpy of fusion (J/g)	Melting temperature (°C)	$x_c$	a-axis crystal thickness (nm)	$x_c$	C7 FWHM (Hz)
Fast	8.9 ± 0.6	230	0.46	24	0.47	50
Slow	21 ± 2	245	0.62	37	0.55	23

The DSC data is taken from Ref. 17.

The cross polarization (CP) pulse sequence (Fig. S1a) utilizes pulses on both the  $^{13}\text{C}$  and  $^1\text{H}$  channels. Under static conditions, polarization transfer is optimal when the  $B_1$  fields of the  $^1\text{H}$  and  $^{13}\text{C}$  resonances match ( $B_{1\text{H}}=B_{1\text{C}}$ ), which is the so-called 'Hartman–Hahn match'. However, under MAS, this condition becomes perturbed because the  $^1\text{H}$ – $^{13}\text{C}$  and  $^1\text{H}$ – $^1\text{H}$  dipolar couplings become time dependent, causing the local  $^1\text{H}$  fields to be frequency and amplitude modulated.<sup>[19]</sup> As a result, CP kinetics depends on local proton density and organic functionality, as was shown in previous works.<sup>[20,21]</sup> CP transfer is complicated further in highly motionally averaged  $^1\text{H}$  spin systems, such as the hexyl side-chain protons of P3HT, so one must be careful to ensure that relative peak intensities in the spectrum are proportional to the mole fraction of  $^{13}\text{C}$ , and hence meaningful. In order to explore the impact of CP conditions on the  $^{13}\text{C}$  NMR intensity, CPMAS spectra were taken as a function of MAS rate, temperature, CP time, and Hartmann–Hahn matching field strength ( $B_1$ ).

In Fig. 2, we have plotted CPMAS signal intensity with respect to  $^1\text{H}$   $B_1$  field (while keeping the  $^{13}\text{C}$   $B_1$  field fixed) for spectra taken on the fast-dried film at room temperature with two different MAS rates. The y-axes in Fig. 2 are proportional to the CP rate. At slow MAS rates, the strongly coupled thiophene carbon (C8) displays a broad distribution of  $B_{1\text{H}}$  matching values (Fig. 2a), whereas the nonprotonated carbons (Fig. 2b) display sharper peaks at integers of the MAS frequency ( $B_{1\text{H}}=B_{1\text{C}}\pm n\cdot\nu_r$ ,  $\nu_r=4.9$  kHz) very similar to the first CPMAS experiments on adamantane,<sup>[18]</sup> which is a highly dynamic, weakly coupled solid. Importantly, maxima occur for both protonated and nonprotonated carbons alike at the  $B_{1\text{H}}$  fields offset by one unit of the spinning frequency ( $B_{1\text{H}}=B_{1\text{C}}\pm 1\cdot\nu_r$ ), indicating that these  $B_{1\text{H}}$  fields are good CP conditions for all of the carbons in P3HT, increasing the likelihood for quantitation. Similar profiles for the side-chain carbons are given in Fig. S2.

When spinning at 9.8 kHz, however, the matching conditions change dramatically (Fig. 2c and d). The protonated thiophene carbon exhibits a fast CP rate at  $B_{1\text{H}}=B_{1\text{C}}$ , as indicated by the large peak at 57 kHz (Fig. 2c). However, the nonprotonated thiophene carbons exhibit *attenuated* CP transfer at that same condition (small peak at 57 kHz in Fig. 2d). At  $B_{1\text{H}}$  values offset by one unit of the MAS frequency (47.2 and 66.8 kHz), however, these situations are reversed: The protonated thiophene carbon exhibits smaller peaks and the nonprotonated carbons bigger. *The result is that at faster MAS rates, it becomes increasingly difficult to find a single set of optimal  $B_{1\text{H}}$  and  $B_{1\text{C}}$  values for all of the thiophene carbons in P3HT because of the diversity of couplings that exist.* Lower spinning rates (<5 kHz) will generally allow for a greater number of good Hartmann–Hahn matching conditions for P3HT. The absence of an adequate CPMAS condition at faster MAS rates is a result of the presence of both strong and weak  $^1\text{H}$ – $^{13}\text{C}$  couplings (the C8 and C7, C9, C10, respectively) and slow  $^1\text{H}$ – $^1\text{H}$  spin exchange. The presence of weak  $^1\text{H}$ – $^1\text{H}$  couplings is suggested in the motionally narrowed SPE  $^1\text{H}$  NMR spectrum (19 kHz FWHM). The square root of the  $^1\text{H}$ – $^{13}\text{C}$  second moment is expected to be ca. <5 kHz.

To investigate the impact of the  $^1\text{H}$ – $^{13}\text{C}$  and  $^1\text{H}$ – $^1\text{H}$  coupling strengths on CPMAS efficiency, we acquired CPMAS spectra as a function of the  $^1\text{H}$   $B_1$  field at lower temperatures (–40 °C) where the couplings are much stronger ( $\approx 40$  kHz FWHM); the square root of the  $^1\text{H}$ – $^{13}\text{C}$  second moment is expected to be  $\approx 10$  kHz. As shown in Fig. 2e and f, the peaks in the Hartmann–Hahn profiles for the protonated (Fig. 2e) and nonprotonated (Fig. 2f) carbons overlap much better at –40 °C even when spinning at 9.8 kHz. In fact, spinning at 4.9 kHz does little to improve the uniformity of the matching conditions (data not shown).

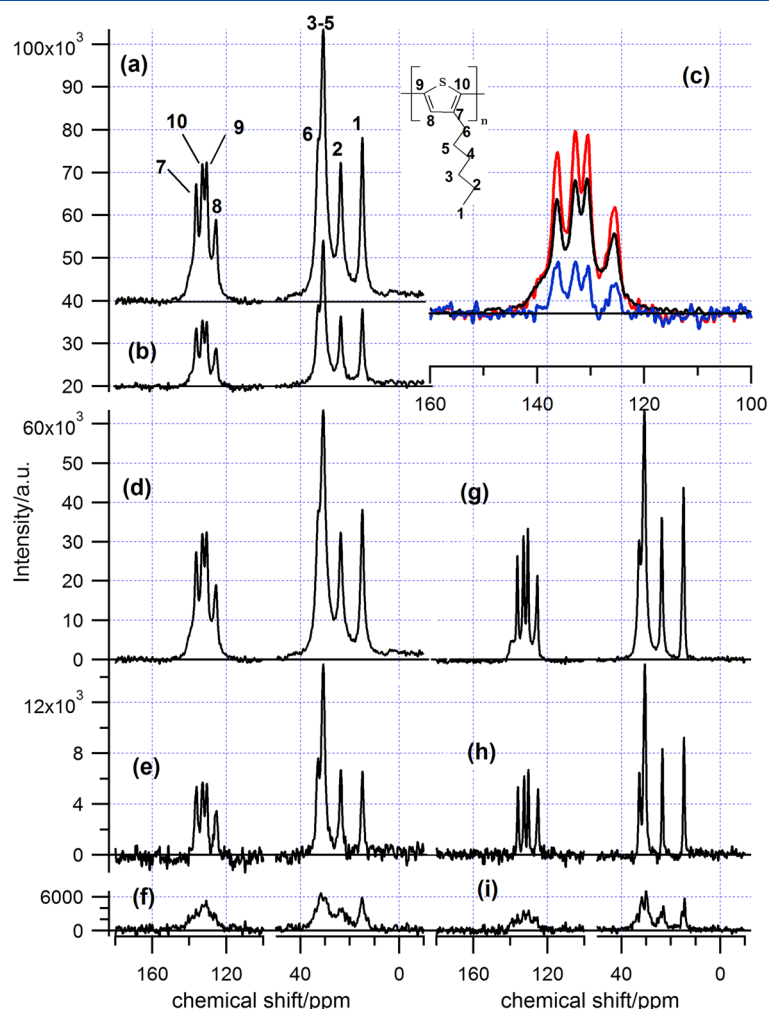


**Figure 1.** (a)  $^{13}\text{C}$  cross-polarization magic angle spinning (CPMAS) nuclear magnetic resonance spectrum of fast-dried P3HT film, including the assignments of the ten carbons on the monomer both without (a) and with (b) a 7 ms pre-spinlock filter. (c) A zoom-in of the thiophene spectral region of the CPMAS spectrum with the pre-spinlock pulse (red), the CPMAS spectrum scaled by 0.35 (black), and the difference (blue). CPMAS spectra for fast-dried poly(3-hexylthiophene) (P3HT) (d) and its ordered (e) and disordered fractions (f). CPMAS spectra for slow-dried P3HT (g) and its ordered (h) and disordered (i) fractions.

In principle, one could attempt ramping the CP condition.<sup>[22]</sup> However, we found it difficult to reproduce quantitative peak heights, even after many trials of synthesized ramping conditions. In light of these results, we generally recommend spinning at slower MAS rates if one is interested in being quantitative with the  $^{13}\text{C}$  CPMAS spectrum of P3HT at room temperature. For those investigating other semiconducting polymers with, perhaps, varied side-chain length or branched side chains, a simple check of the  $^1\text{H}$  NMR resonance should roughly inform what MAS rate to use ( $\nu_r < \text{FWHM}/4$ ).

Once a Hartman–Hahn match is found, one must choose the correct CP time. Because CP rate is proportional to the strength of the  $^1\text{H}$ – $^{13}\text{C}$  dipolar coupling, the CP rates will vary considerably amongst carbon sites in light of the variability of couplings present. Furthermore, the CPMAS intensity will decay with rate  $1/T_{1\rho}^{\text{H}}$ , so, because  $T_{1\rho}^{\text{H}}$  heterogeneity can exist, an optimal CP time should be chosen so as to minimize any differential  $T_{1\rho}^{\text{H}}$  effects. In order to explore the CP kinetics, CPMAS spectra were acquired at 2.3 T ( $\nu_{\text{MAS}} = 3.8 \text{ kHz}$ ) as a function of CP time; the intensities of the resonances are plotted as a function of CP time in Fig. 3. As shown in the figure, all of the resonances do in fact build up at different rates but are all greater than 93% of the expected

maximum intensity between 1.5 and 2.5 ms. Cross polarizing at shorter times gives rise to diminished intensity in the nonprotonated carbons (130, 133, 136 ppm), and CPMAS with longer times gives rise to diminished intensity of the broader features with shorter  $T_{1\rho}^{\text{H}}$ . To illuminate the quantitative nature of CPMAS at low speed MAS (<5 kHz) and with a 2 ms contact time, a comparison between a CPMAS spectrum taken with these conditions and a  $^{13}\text{C}$  SPE NMR spectrum (i.e. the quantitative ‘gold standard’) is given in Fig. 4 along with the residual. The negligible intensity (<4% integral) in the residual spectrum demonstrates the similarity of the CPMAS and SPE spectra, ultimately showing that one can acquire quantitative CPMAS spectra at room temperature in P3HT when spinning at lower MAS rates (<5 kHz) and using a 2.0 ms contact time.

### $^{13}\text{C}$ CPMAS NMR spectral editing and crystallinity determination

$^{13}\text{C}$  CPMAS spectra were taken at room temperature on two P3HT films in order to assess their degree of crystallinity. Because the narrow thiophene resonances represent crystalline polymer chains, we performed  $T_{1\rho}^{\text{H}}$ -filtered (spectral editing) CPMAS experiments in an

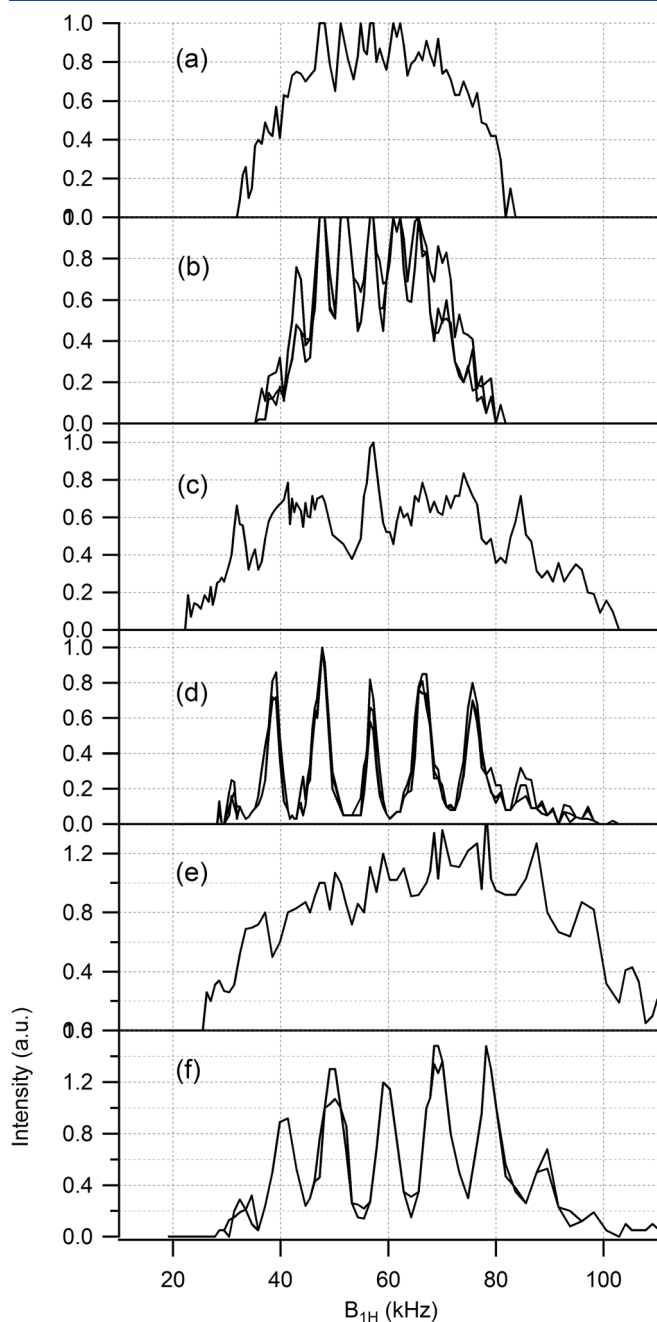


**Figure 2.** Plots of CPMAS intensity of the protonated (a),(c),(e) and nonprotonated (b),(d),(f) thiophene carbons as a function of the  $^1\text{H}$   $B_1$  field under the following conditions: (a) 4.9 kHz magic angle spinning (MAS), 25 °C; (b) 4.9 kHz MAS, 25 °C; (c) 9.8 kHz MAS, 25 °C; (d) 9.8 kHz MAS, 25 °C; (e) 9.8 kHz,  $-40^\circ\text{C}$ ; and (f) 9.8 kHz,  $-40^\circ\text{C}$ . The contact time was 3 ms. At 25 °C,  $B_{1C} = 57$  kHz, and at  $-40^\circ\text{C}$ ,  $B_{1C} = 59$  kHz.

effort to separate the spectrum into its crystalline and noncrystalline components; the pulse sequence of the  $T_{1\rho}^H$ -filtered CPMAS experiment is given in Fig. S1b. The important characteristic of  $T_{1\rho}^H$  is that it is a *locally* homogenized relaxation time because of  $^1\text{H}$  spin diffusion. The duration of the spin-lock pulse was chosen to be long enough (7 ms) to produce complete spin equilibration over a given monomer unit (or multiple monomer units) to ensure that all the protons on a given monomer unit exhibit the same  $T_{1\rho}^H$ , depending only on mesophase (i.e. crystal or noncrystal). The size scale of relaxation time averaging,  $x$ , goes as  $x = \sqrt{4Dt}$ , where  $D$  is the spin

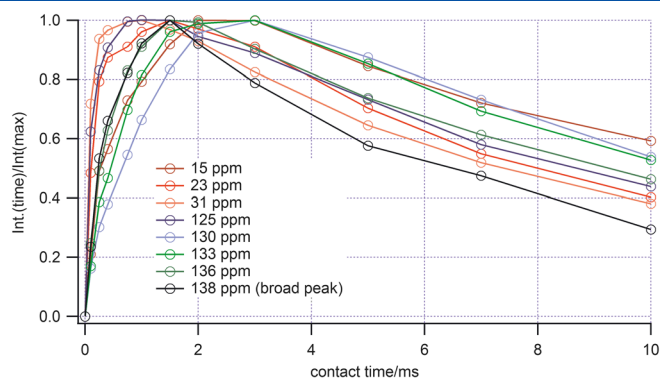


**Figure 3.** Plot of CPMAS intensity for various cross polarization times at 293 K and 2.35 T.

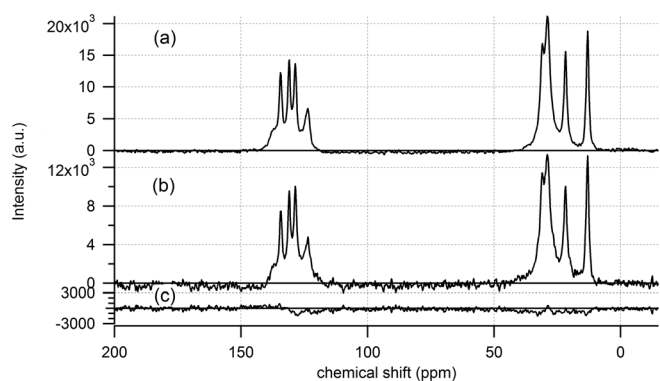


**Figure 4.** CPMAS spectrum (a), single pulse excitation  $^{13}\text{C}$  spectrum (b), and the difference spectrum (c) of a P3HT film at 2.35 T. The single pulse excitation  $^{13}\text{C}$  NMR was acquired with recycle delays  $>5 \cdot T_1$ . Other pertinent experimental details are in the 'Experimental' section in the succeeding texts. The  $T_1$ 's of fast-dried P3HT, which were measured with the Torchia sequence, (i) are given in the Supporting Information.

diffusion coefficient ( $\approx 0.2\text{--}0.4 \text{ nm}^2/\text{ms}$  for P3HT),<sup>[23]</sup> and  $t$  is the length of the spin-lock pulse. A 7 ms spin-lock pulse would correspond to a 2 to 3 nm domain, which certainly encompasses a monomer unit of P3HT but is smaller than the crystal.

An example of the spectral editing procedure is given in Fig. 1. The CPMAS spectrum (no relaxation filter) is given in Fig. 1a, and the  $T_{1\rho}^H$ -filtered CPMAS spectrum is given in Fig. 1b. The intensities are to scale, so one observes that all the resonances have decayed because of the filter but at different rates depending on resonance position. The broader resonances have decayed faster than the narrower resonances. We have included a zoom-in of the thiophene spectral region to illuminate this point, which displays the CPMAS spectrum (black, scaled by 0.35), the  $T_{1\rho}^H$ -filtered CPMAS spectrum (red), and their difference (blue). As shown from Fig. 1c, the broad downfield shoulder at 138 ppm in both spectra overlaps, indicating that the glassy sites have decayed to 0.35 of their original value. The peaks of the narrower resonances are much higher as a result of the longer  $T_{1\rho}^H$ . In Fig. 1c, we include the difference, [(blue) = (red) – (black)], which exhibits no appreciable intensity at 138 ppm, allowing us to attribute this spectrum to crystalline P3HT. The full crystal spectrum of the fast-dried film is given in Fig. 1e, and that of the noncrystal is given in Fig. 1f. The slow-dried film's crystal and noncrystal spectra are given in Figs. 1h and 1i, respectively. The crystalline fractions (i.e. crystallinities), which are calculated by  $x_c = \frac{I_{\text{xtal}}}{I_{\text{xtal}} + I_{\text{non-xtal}}}$  are given in Table 1 (right side), where  $I_{\text{xtal}}$

and  $I_{\text{non-xtal}}$  are the integrated intensities of the crystal and noncrystal CPMAS spectra, respectively.

The quantitative nature of this technique is gleaned from the fact that the resonances of *all* ten carbons of P3HT have intensity values that approximately relate to their absolute  $^{13}\text{C}$  fraction. This holds for both samples – crystal and noncrystal. Because of complete  $^1\text{H}$  spin equilibration on a given monomer site, all of the protons on a given monomer unit (as observed by their cross-polarized carbons) have the same effective  $T_{1\rho}^{\text{H}}$ . If the spin equilibration across the entire monomer unit had not occurred (i.e. the monomer unit was  $>3$  nm or the side chain was more highly dynamic and  $D < 0.2$  to  $0.4$  nm<sup>2</sup>/ms), then the peak intensities would not necessarily be quantitative.

Deconvoluting the  $^{13}\text{C}$  CPMAS spectra allows us to comment on differences in line shapes depending on mesophase as well as a prospect that could be useful for investigating correlations between molecular conformation, crystal size, and paracrystallinity. For instance, the resonances of the slow-dried film's crystal fraction (Fig. 1h) are notably narrower than its fast-dried counterpart (Fig. 1e), suggesting differences in molecular conformations. The full width at half maximum (FWHM) of the 136 ppm resonance (C7) of the fast-dried film is 50 Hz (2.0 ppm); the C7 resonance of the slow-dried film is 23 Hz (0.9 ppm) broad. Because the fast-dried film's crystals are smaller by approximately a factor of two (Table 1, DSC data), one might expect the conformations of crystalline chains in the fast dried film to be less uniform because the population of chains closer to the crystal surface (where chains could become more highly disordered) is greater. The C7 carbon is a good reporter of conformation because (i) the nonprotonated carbons have less relative  $1/T_{2\text{C}}$  broadening, making them less susceptible to variations in  $^1\text{H}$ - $^{13}\text{C}$  decoupling; and (ii) there is greater spectral separation from the other nonprotonated thiophenes (C9, C10).

### Variable temperature $^1\text{H}$ NMR

While  $T_{1\rho}^{\text{H}}$  spectral editing may work for P3HT, how easily could it be extended to other semiconducting polymers? Are there other relaxation times that could also be used for deconvoluting the crystalline from the noncrystalline spectra? It has been shown that the crystallinities of classic polymers such as polyethylene and polypropylene can be quantified when using  $T_2^{\text{H}[24]}$  and  $T_{1xz}^{\text{H}[25]}$  relaxation time differences, respectively, so in order to explore whether other relaxation times could be used for spectral editing, we performed  $^1\text{H}$  SPE (i.e. linewidth),  $T_{1\rho}^{\text{H}}$ , and  $T_{1xz}^{\text{H}}$  NMR experiments as a function of temperature. The pulse sequences are given in Fig. 5. The side chains contain 93% of P3HT's protons, so  $^1\text{H}$  relaxation experiments report essentially on local side-chain dynamics and packing. As we have shown in the succeeding texts, this characteristic proves to serve as the principle roadblock for using these relaxation times for quantifying order.

### $^1\text{H}$ NMR linewidths

The FWHM of the  $^1\text{H}$  NMR resonance is a measure of molecular packing and chain dynamics, mostly on the (0.01 to 1 ms) timescale<sup>[26]</sup> and has classically been utilized to determine crystallinity in polyethylene.<sup>[27]</sup> In the presence of large amplitude molecular motions, the  $^1\text{H}$  resonance becomes narrower than its theoretical maximum breadth primarily because of increases in  $T_{2\text{H}}$ , the  $^1\text{H}$  spin-spin relaxation time (i.e.  $\text{FWHM} \propto (T_{2\text{H}})^{-1}$ ). At a given temperature, a broader  $^1\text{H}$  resonance (and shorter  $T_{2\text{H}}$ ) is expected to arise from more tightly packed, denser regions of

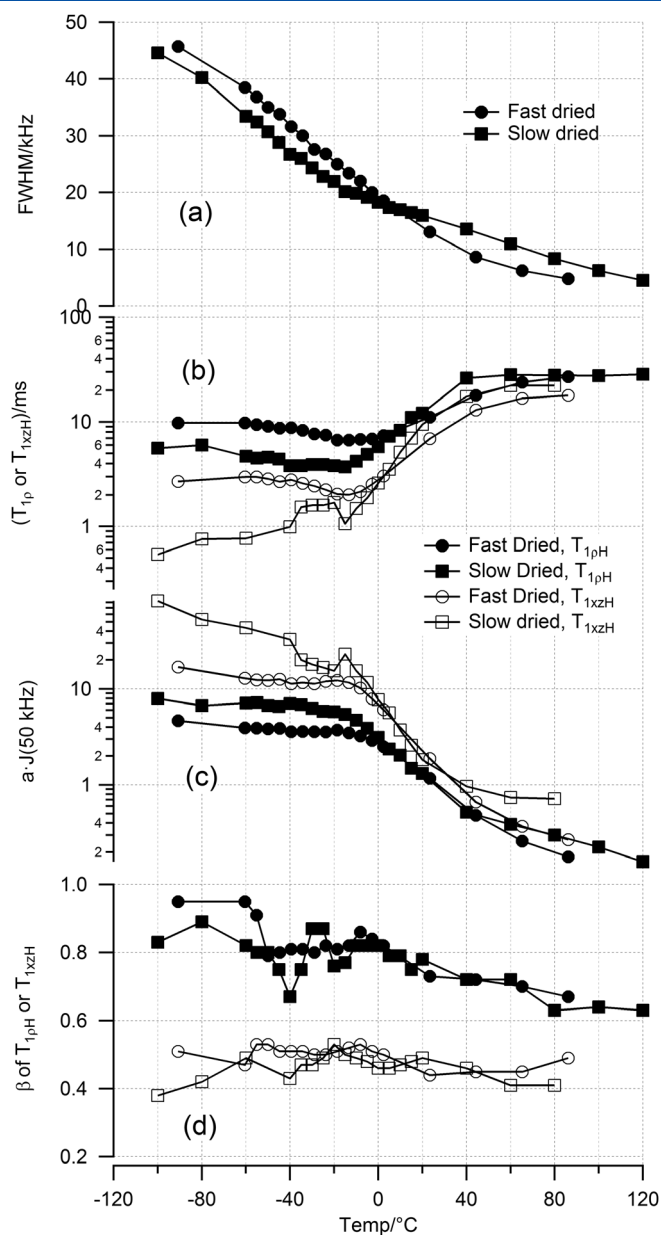


**Figure 5.**  $^1\text{H}$  NMR data taken at 7.05 T for various temperatures. (a) FWHM of the  $^1\text{H}$  single pulse excitation spectra, (b)  $T_{1\rho}^{\text{H}}$  and  $T_{1xz}^{\text{H}}$  relaxation times, (c) 50 kHz spectral density parameter, and (d) the dispersion parameter,  $\beta$ , for  $T_{1\rho}^{\text{H}}$  and  $T_{1xz}^{\text{H}}$ .

protons, and a narrower line is expected for regions of looser packing. In Fig. 5a, we have plotted the  $^1\text{H}$  NMR FWHM as a function of temperature for both P3HT films. As shown from the plot,  $^1\text{H}$  NMR resonances from both films narrow significantly upon heating demonstrating that on average the hexyl side chains are quite mobile and approximately melted at temperatures greater than  $-100$  °C. Side-chain mobility is evident over the entire temperature range investigated ( $-100$  to  $120$  °C) because the low temperature plateau has not yet been reached at  $-100$  °C. Despite the prevalence of side-chain mobility, the modest FWHM values ( $>1$  kHz) observed indicate that the side chains are not isotropically reorienting on the  $\approx 1$  ms timescale even at temperatures  $>50$  °C, which is a result of the side chains being tethered.

While it is true that the  $^1\text{H}$  NMR resonances include signals from both the crystalline and noncrystalline regions, the FWHM changes

in each sample are monotonically changing. Hence, motions of the side chains in the crystalline and noncrystalline regions appear to change gradually with temperature and with similar profiles. Furthermore, linewidths taken at different points on the  $^1\text{H}$  NMR resonances (e.g. full width at 1/4 maximum and full-width at 3/4 maximum) reveal similar profiles as Fig. 5a. These data are given in Fig. S3. Overall, this would suggest that there is only little  $T_2$  contrast between the crystal and noncrystal, making it a poor candidate for crystal *versus* noncrystal spectral editing. Furthermore,  $T_2$  is not a spin-diffusion-averaged relaxation time, and there can potentially be *distributions* of  $T_2$  on a given side chain of P3HT. We do observe, however, *subtle* differences in the FWHM profiles for both films, suggesting that  $T_2$  is slightly dependent on polymer order, although the relationship is not seemingly straightforward (refer to succeeding texts). We comment on two observations, which could be helpful in future interrogations of the side-chain dynamics of P3HT.

First, the fast-dried film (black dots) exhibits a broader line than the slowly dried film in the temperature range of  $-100$  to  $0^\circ\text{C}$ , which implies a more spatially restrictive packing of side chains on average despite the lower crystallinity. In our previous low temperature  $^{13}\text{C}$  CPMAS experiments,<sup>[16]</sup> we observed greater populations of anticonformers in less crystalline P3HT, indicating more rigid side chains. The side-chain packing in noncrystalline regions could be expected to be slightly improved over the crystal, because the alkyl chains will have more freedom for improved packing. Similar behavior was observed in melt-quenched regiorandom P3HT, in which nanophase separation was driven by the alkyl side chains.<sup>[28]</sup> Ultimately, the crystal structure is a compromise between free-energy optimization of the backbone *versus* the side-chain packing, it being unlikely that a single structure would simultaneously optimize both. Because the most dominant interactions driving the crystallization are the  $\pi$ - $\pi$  forces experienced by the backbone, the crystal structure is probably closer to optimizing main chain packing, not side-chain packing.

Secondly, while the fast-dried film displays a seemingly monotonic decrease in FWHM with temperature (Fig. 5a, filled circles), which would generally be associated with a continuous melting of side chains (greater amplitudes and/or higher frequency motions), the FWHM of the slowly dried film exhibits a sharp change to more gradual slope at approximately  $-15^\circ\text{C}$ . At temperatures greater than  $10^\circ\text{C}$ , the slowly dried film then exhibits greater FWHM values than does the fast-dried film. This change to more gradual slope suggests that chains in the larger and better-formed crystals of the slow dried film are able to restrict the overall side-chain motions to a degree higher than that for the fast-dried sample at temperatures  $>10^\circ\text{C}$ . At this point, we do not know the exact physical interpretation of the change in slope. We do, however, speculate that it is a result of either a structural or dynamic transition in the crystalline regions.

### $T_{1p}^H$ and $T_{1xz}^H$ relaxation

The polymer packing was also investigated from the  $T_{1p}^H$  and  $T_{1xz}^H$  measurements, which are relaxation times sensitive to dynamic fluctuations in the mid-kHz spectral regime and have been utilized to determine crystallinity in cellulose<sup>[29]</sup> and polypropylene, respectively.<sup>[23]</sup>  $T_{1p}^H$  and  $T_{1xz}^H$  both report on fluctuations in similar frequency ranges, but including both measurements offers the advantage of probing mid-kHz fluctuations with and without the influence of spin diffusion, because spin diffusion is minimized during the acquisition of  $T_{1xz}^H$ .<sup>[30]</sup> A comparison of  $T_{1p}^H$  and  $T_{1xz}^H$  times,

then, offers the opportunity of measuring the length scales of dynamic heterogeneities, because common  $T_{1p}^H$  times (milliseconds) are generally averaged by spin diffusion over spin clusters that can span a few nanometers, depending on the  $T_{1p}^H$  value. Recall from the preceding texts that the size scale of the  $T_{1p}^H$  relaxation time averaging,  $x$ , goes as  $\sqrt{4Dt}$ , which for P3HT is approximately 2 to 3 nm. Again, the size scales of these heterogeneities are important, because meaningful crystallinity quantitation via spectral editing hinges on there being relaxation time differences on size scales smaller than the crystal size but greater than a monomer repeat unit.

The  $T_{1p}^H$  and  $T_{1xz}^H$  times are plotted as a function of temperature in Fig. 5b as the closed and open symbols, respectively; the distribution breadths of the relaxation times, which are described by  $\beta$ , are given in Fig. 5d. The  $\beta$  value, which ranges from 0 to 1 with lower values indicating broader distributions, is the exponent of the stretched exponential function describing the decay curve. Upon inspecting the  $T_{1p}^H$  time breadth (Fig. 5d, filled symbols), one observes the  $\beta$  values (0.6 to 0.95). Recall that all of the protons on a monomer size will exhibit essentially the same  $T_{1p}^H$  because of relaxation time averaging. The  $T_{1xz}^H$   $\beta$  values (Fig. 5d, open symbols) are lower ( $\beta \approx 0.5 \pm 0.1$ ), corresponding to a greater spread in relaxation times. Recall that negligible relaxation time averaging occurs in  $T_{1xz}^H$  so different protons within a given monomer will only exhibit the same  $T_{1xz}^H$  time if the molecular dynamics are similar. The  $T_{1xz}^H$  distribution breadth will *only* match that of  $T_{1p}^H$  if there is no local dynamic heterogeneity, which is not observed; the  $T_{1xz}^H$  breadth is much greater. Hence, significant dynamic heterogeneity must exist on  $<3$  nm size scales, which is not surprising because one may expect, for instance, sites toward the side-chain end (i.e. protons on C2) to be more highly dynamic than sites closer to the main chain (i.e. protons on C5). Hence,  $T_{1xz}^H$  is not a good candidate for crystal *versus* noncrystal spectral editing of P3HT because there are distributions of  $T_{1xz}^H$  times within a monomer. However,  $T_{1xz}^H$  does hold promise for investigating the molecular dynamics on intramonomer size scales, particularly if '100% crystalline' or '100% noncrystalline' samples can be made.

$T_{1p}^H$  and  $T_{1xz}^H$  both depend on the amplitude and timescale of motion, which affect the local field strength and spectral density, respectively. In order to roughly isolate these effects, we have

plotted the relaxation rate-to-FWHM ratio,  $\frac{1}{T_{1p}^H} \frac{1}{FWHM}$  or  $\frac{1}{T_{1xz}^H} \frac{1}{FWHM}$ , which should be proportional to the spectral density at the nutation frequency,  $J(50\text{ kHz})$ . In this case, the FWHM, which is proportional to the second moment of the  $^1\text{H}$  line, serves to normalize the relaxation rate by the expected local field and is temperature dependent. While this relation is not strictly correct, it simply serves as an approximation to disentangle the effects of the local field strength and spectral density, both of which contribute to  $T_{1p}^H$  and  $T_{1xz}^H$ . By inspection of Fig. 5c, one observes that from  $-100$  to ca.  $-10^\circ\text{C}$ , both films exhibit little change in  $J(50\text{ kHz})$ , and the fast dried film is slightly lower. At temperatures  $>ca. -10^\circ\text{C}$ , the curves of both films overlap and show a similar drop in  $J(50\text{ kHz})$  because the side-chain fluctuations have entered the fast fluctuation limit ( $t_c < 1/\omega_1 = 0.1\text{ ms}$ ). These data demonstrate that the three  $^1\text{H}$  NMR parameters (FWHM,  $T_{1p}^H$  and  $T_{1xz}^H$ ) are all linked by the interplay of nearest neighbor packing and rigidity and their impact on available free volume for the side-chain motion which influences amplitudes of motions. Because the available free volume is so critical in its influence on the amplitude of motion (which primarily influences FWHM values), packing differences will generally show up

as differences in  $T_{1\rho}^H$  or  $T_{1xz}^H$ . The important result is that differences in  $T_{1\rho}^H$  times can be used for distinguishing between crystalline and noncrystalline P3HT despite approximately similar spectral densities at  $\omega_1 = 50$  kHz. Extensions of  $T_{1\rho}^H$ -based spectral editing to other semiconducting polymers may or may not follow the same trend as P3HT, but  $T_{1\rho}^H$  shows promise as a spectral filter because of spin diffusion averaging effects and the fact that dynamic heterogeneity (varied  $T_{1\rho}^H$  times) will likely be accompanied by structural heterogeneity (varied order). For instance, at ca.  $-20^\circ\text{C}$ , ordered P3HT actually exhibits *shorter*  $T_{1\rho}^H$  times than less ordered P3HT, yet there is still contrast. The exact correlation is polymer-specific owing to the molecular dynamics of the side chains.

Encouraged by our  $T_{1\rho}^H$ -based spectral editing with  $^{13}\text{C}$  NMR detection, we performed similar experiments but with  $^1\text{H}$  NMR detection. The experiments were performed at various temperatures for both films in an attempt to deconvolve the  $^1\text{H}$  NMR spectra into components that could be related to something structural (i.e. rigid vs mobile) because, from the relaxation data described in the preceding texts, we knew that the  $T_{1\rho}^H$  times and  $^1\text{H}$  NMR linewidths are correlated. However, these deconvolutions were not successful because both the  $^1\text{H}$  NMR line shapes and the relative intensities of the isolated components were found to change with temperature for both films, which, unlike the more highly resolved  $^{13}\text{C}$  CPMAS spectra, were ambiguous. Without further knowledge of what the '100% crystal'  $^1\text{H}$  NMR line shape should be and how it should change with temperature, such analyses were riddled with ambiguity. These ambiguities have prevented us from commenting on the observed increase in the distribution of  $T_{1\rho}^H$  times (decreasing  $\beta$  values, Fig. 5d) upon increasing temperature, which deceptively would simply be related to heterogeneous side-chain melting dynamics, which is an area of interest to the OE community.<sup>[6,31,32]</sup> However, complicating matters is the inconsistent and unpredictable variation in the  $^1\text{H}$  spin diffusion radius being probed with  $T_{1\rho}^H$  over the temperatures investigated; a monotonic decrease in the spin diffusivity upon heating is anticipated, but the longer  $T_{1\rho}^H$  times observed at higher temperatures serve to increase the spin diffusion radius in a nonlinear fashion (recall  $x = \sqrt{4Dt}$ ). Furthermore, because both the  $T_{1\rho}^H$  and spin diffusivity can vary from domain to domain ( $>2$  to  $5$  nm) and change with temperature, any further interpretations of the relaxation data were not feasible.

## Conclusions

We demonstrated that solid-state  $^{13}\text{C}$  CPMAS NMR can be used for quantifying crystallinity in high molar mass P3HT. Quantitative CPMAS spectra of P3HT can be acquired when using slow MAS rates ( $<5$  kHz) and  $1.5$  to  $2.5$  ms contact times. By use of  $T_{1\rho}^H$ -based spectral editing, the P3HT  $^{13}\text{C}$  NMR spectrum can be deconvolved into its crystalline and noncrystalline components; the relative integrated intensities are used for determining the crystallinity. Sample to sample variations in linewidths were observed in the  $^{13}\text{C}$  CPMAS spectra of crystalline P3HT. These variations are likely a result of differences in crystallization kinetics and, ultimately, a result of differences in chain conformations.

A subtle phase transition involving side-chain dynamics in crystalline P3HT was observed from  $^1\text{H}$  NMR measurements at  $-15^\circ\text{C}$ . Otherwise, the connection between  $T_2$  and main chain order is not obvious because the side chains are highly dynamic in both the crystal and noncrystal. Dynamic contrast is sufficient for  $T_{1\rho}^H$ -based  $^{13}\text{C}$  CPMAS spectral editing but not sufficient for  $T_{12}^H$ ,  $T_{1\rho}^H$ , or  $T_{1xz}^H$ -based spectral editing with  $^1\text{H}$  detection, which has

generally been used for determining crystallinity in classic polymers such as polyethylene.  $T_{1\rho}^H$  and  $T_{1xz}^H$  relaxation experiments showed dynamic heterogeneity over several size scales ( $<2$  and  $>5$  nm) over the entire temperature range investigated ( $-100$  to  $100^\circ\text{C}$ ), which complicates the interpretation of the side-chain dynamics in terms of motional rates and amplitudes via BPP theory.

## Experimental

### Materials

P3HT (Plexcore 2100, Plextronics Inc., Pittsburgh, PA, USA) was used as received. According to the manufacturer, the P3HT is ultra-high purity ( $<25$  ppm trace metals) and highly regioregular ( $>98\%$  head-to-tail), with a number averaged molar mass of  $64500$  g/mol and polydispersity index of  $\leq 2.5$ . The slow-dried film was prepared by drop casting a  $15$  mg/ml solution of P3HT in chlorobenzene into a Teflon well plate; films formed in approximately  $4$  to  $6$  h. The fast-dried film was prepared by drop casting a  $15$  mg/ml solution of P3HT in chloroform ( $>99.8\%$ ) onto a  $70^\circ\text{C}$  heated Teflon substrate; films formed in  $<5$  s. The chloroform ( $>99.8\%$ ) and chlorobenzene ( $>99.8\%$ ) were used as received. The films were sliced into approximately  $50$  fine flakes of  $\approx 0.1$  mm dimension and (lightly) pressed into disks to ensure isotropy and homogeneity in the NMR experiments.

### NMR characterization

Solid-state NMR experiments that were performed at  $7.05$  T on a Bruker DMX300 spectrometer utilizing a  $4$  mm triple resonance magic angle spinning probe. Each sample ( $\approx 30$  mg) was pressed into a  $4 \times 4$  mm disk and placed into a  $4$  mm  $\text{ZnO}_2$  rotor and spun at  $9800$  or  $4900 \pm 1$  Hz. CPMAS NMR experiments were performed under the following conditions:  $75.46$  MHz  $^{13}\text{C}$  frequency,  $300.13$  MHz  $^1\text{H}$  frequency,  $3.2 \mu\text{s} \pi/2$   $^1\text{H}$  excitation pulse,  $2$  to  $3$  ms contact time,  $52$  kHz  $^{13}\text{C}$  contact pulse,  $62$  or  $57$  kHz  $^1\text{H}$  contact pulse,  $78$  kHz TPPM  $^1\text{H}$  decoupling,  $1024$  data points with  $64$   $512$  zero filling points,  $4096$  scans,  $20 \mu\text{s}$  dwell time, and  $5$  s recycle delay. The  $^1\text{H}$  TPPM decoupling<sup>[33]</sup> had the following parameters:  $2$  ppm  $^1\text{H}$  frequency (from TMS),  $170^\circ$  flip angle, and  $15^\circ$  modulation angle. The Hartmann–Hahn match was optimized on crystalline powders of adamantane, which was also served for calibration of the  $^{13}\text{C}$  frequency scale (adamantane  $\text{CH}_2$  set to  $38.5$  ppm).<sup>[34]</sup>

The  $^1\text{H}$  relaxation NMR experiments were performed on a  $5$  mm Doty Combined Rotation And Multiple Pulse probe at  $300$  MHz.  $^1\text{H}$  single pulse excitation experiments had the following conditions:  $1.5 \mu\text{s} \pi/2$  pulse,  $1 \mu\text{s}$  dwell time,  $16$  scans,  $1024$  data points with  $64$   $512$  zero filling points, and  $5$  s recycling delay.  $^1\text{H}$  free induction decays were acquired within  $4 \mu\text{s}$  of the  $^1\text{H} \pi/2$  pulse, and the first two data points were left shifted prior to the Fourier transform. The  $T_{1\rho}^H$  experiments were performed with the same conditions, but with a variable time of  $50$  kHz spin lock pulse immediately after  $^1\text{H}$  excitation. The  $T_{1xz}^H$  experiments, which utilize stroboscopic detection under  $^1\text{H}$  homonuclear decoupling, were performed with the MREV-8 pulse sequence,<sup>[35]</sup> with the following parameters: eight  $1.5 \mu\text{s} \pi/2$  pulses, cycle time  $39.6 \mu\text{s}$ ,  $1400$  data points, and  $8$  s recycle delay. The plotted  $T_{1\rho}^H$  times (Fig. 5) were taken to be the fit of the NMR signal intensity as a function of  $50$  kHz spin-lock pulse time. The data were fit to a stretched exponential so as to ascertain an estimate of the dispersion ( $\beta$ ) of the relaxation times as well. The  $T_{1xz}^H$  times (Fig. 5) were taken to be the fit of the intensity

during MREV-8 irradiation under spin-locked nonspinning conditions, and the data were fit to a stretched exponential as well.

The variable temperature experiments were performed using a liquid nitrogen heat exchanger with nitrogen drive gas. Temperatures for the CPMAS were calibrated with  $^{207}\text{Pb}$  magic angle spinning NMR spectra on an internal standard of lead nitrate.<sup>[36]</sup> Temperatures for the  $^1\text{H}$  relaxation experiments were calibrated with  $^1\text{H}$  NMR experiments on external standards of methanol and propylene glycol.<sup>[37,38]</sup> All temperatures quoted are within  $\pm 3^\circ\text{C}$ . Over the temperature range of these experiments, magic angle spinning  $^{79}\text{Br}$  NMR spectra of KBr show no notable change in line shape or number of spinning sidebands, which indicates that linewidth changes as a function of temperature seen in Fig. 5 are not attributable to deviations from the magic angle. Furthermore, there is no appreciable change in  $^1\text{H}$  decoupling field ( $B_1^H > 70\text{ kHz}$ ) at these lower temperatures.

Solid-state NMR experiments that were performed at 100 MHz (2.35 T) were on a Tecmag Apollo spectrometer, ultrawide bore Nalorac magnet, and home-built 7.5 mm double resonance magic angle spinning probe. Each sample ( $\approx 100\text{ mg}$ ) was pressed into a  $6 \times 7\text{ mm}$  disk, placed into a Magic rotor, and spun at  $3800 \pm 100\text{ Hz}$ . CPMAS NMR experiments were performed with the following conditions: 25.19 MHz  $^{13}\text{C}$  frequency, 100.16 MHz  $^1\text{H}$  frequency,  $3.2\ \mu\text{s}$   $^1\text{H}$   $\pi/2$  pulse, 2 ms contact time, 72 kHz  $^{13}\text{C}$  contact pulse, 68 kHz  $^1\text{H}$  contact pulse, 78 kHz continuous wave (cw) decoupling, 100  $\mu\text{s}$  dwell time, 600 data points with 15 784 zero filling points, 2048 to 8196 scans, and 4 s recycle delay. The  $^1\text{H}$  cw decoupling frequency was set to 2 ppm (relative to tetramethylsilane at 0 ppm).

## Acknowledgements

We acknowledge J. Marino, K. Page, and D. L. VanderHart for their thoughtful comments and edits of this manuscript. D. M. DeLongchamp, C. R. Snyder, and C. S. Soles are acknowledged for their helpful discussions. Certain commercial equipment and materials are identified in this paper in order to specify adequately the experimental procedure. In no case does such identification imply recommendations by the National Institute of Standards and Technology nor does it imply that the material or equipment identified is necessarily the best available for this purpose.

## References

- [1] K. Yawaza, Y. Inoue, T. Yamamoto, N. Asakawa. *Phys. Rev. B* **2006**, *74*, 094204. doi:10.1103/PhysRevB.74.094204.
- [2] K. Yazawa, Y. Inoue, T. Shimizu, M. Tansho, N. Asakawa. *J. Phys. Chem. B* **2010**, *114*, 1241–1248. doi:10.1021/jp910590d.
- [3] C. Yang, J. G. Hu, A. J. Heeger. *J. Am. Chem. Soc.* **2006**, *128*, 12007–12013. doi:10.1021/ja063707f.
- [4] R. Mens, F. Demir, G. Van Assche, B. Van Mele, D. Vanderzande, P. J. Adriaensens. *J. Poly. Sci. A: Poly. Chem.* **2012**, *50*, 1037–1041. doi:10.1002/pola.25865.
- [5] F. Martini, S. Borsacchi, S. Spera, C. Carbonera, A. Cominetti, M. J. Geppi. *J. Phys. Chem. C* **2013**, *117*, 131–139. doi:10.1021/jp3103904.
- [6] H. Siringhaus, P. J. Brown, R. H. Friend, M. M. Nielsen, K. Bechgaard, B. M. W. Langeveld-Voss, A. J. H. Spiering, R. A. J. Janssen, E. W. Meijer, P. Herwig, D. M. de Leeuw. *Nature* **1999**, *401*, 685–688. doi:10.1038/44359.
- [7] R. A. Street, J. E. Northrup, A. Salleo. *Phys. Rev. B* **2005**, *71*, 165202. doi:10.1103/PhysRevB.71.165202.
- [8] L. H. Jimison, M. F. Toney, I. McCulloch, M. Heeney, A. Salleo. *Adv. Mater.* **2009**, *21*, 1568–1572. doi:10.1002/adma.200802722.

- [9] R. J. Kline, M. D. McGehee, M. F. Toney. *Nature Mater.* **2006**, *5*, 222–228. doi:10.1038/nmat1590.
- [10] J. L. Baker, L. H. Jimison, S. Mannsfeld, S. Volkman, S. Yin, V. Subramanian, A. Salleo, A. P. Alivisatos, M. F. Toney. *Langmuir* **2010**, *26*, 9146–9151.
- [11] E. D. Gomez, K. P. Barteau, H. Wang, M. F. Toney, Y.-L. Loo. *Chem. Commun.* **2011**, *47*, 436–438. doi:10.1039/C0CC02927K.
- [12] J. Clark, C. Silva, R. H. Friend, F. C. Spano. *Phys. Rev. Lett.* **2007**, *98*, 206406. doi:10.1103/PhysRevLett.98.206406.
- [13] L. H. Jimison, S. Himmelberger, D. T. Duong, J. Rivnay, M. F. Toney, A. Salleo. *J. Poly. Sci., B: Poly. Phys.* **2013**, *51*, 611–620. doi:10.1002/polb.23265.
- [14] O. F. Pascui, R. Lohwasser, M. Sommer, M. Thelakkat, T. Thurn-Albrecht, K. Saalwachter. *Macromolecules* **2010**, *43*, 9401–9410. doi:10.1021/ma102205t.
- [15] M. R. Hansen, R. Graf, H. W. Spiess. *Chem. Rev.* **2015** ASAP. doi:10.1021/acs.chemrev.5b00258.
- [16] R. H. Newman, L. M. Condrón. *Solid State Nucl. Magn. Reson.* **1995**, *4*, 259–266. doi:10.1016/0926-2040(94)00047-G.
- [17] R. C. Nieuwendaal, C. R. Snyder, D. M. DeLongchamp. *ACS Macro. Lett.* **2014**, *3*, 130–135. doi:10.1021/mz4005343.
- [18] C. R. Snyder, R. C. Nieuwendaal, D. M. DeLongchamp, C. K. Luscombe, P. Sista, S. D. Boyd. *Macromolecules* **2014**, *47*, 3942–3950. doi:10.1021/ma500136d.
- [19] E. O. Stejskal, J. Schaefer, J. S. Waugh. *J. Magn. Reson.* **1977**, *28*, 105–112. doi:10.1016/0022-2364(77)90260-8.
- [20] L. B. Alemany, D. M. Grant, R. J. Pugmire, T. D. Alger, K. W. Zilm. *J. Am. Chem. Soc.* **1983**, *105*, 2133–2141. doi:10.1021/ja00346a006.
- [21] L. B. Alemany, D. M. Grant, R. J. Pugmire, T. D. Alger, K. W. Zilm. *J. Am. Chem. Soc.* **1983**, *105*, 2142–2147. doi:10.1021/ja00346a007.
- [22] G. Metz, X. Wu, S. O. Smith. *J. Magn. Reson. Adv. Physiol. Educ.* **1994**, *110*, 219–227.
- [23] R. C. Nieuwendaal, H. W. Ro, D. S. Germack, R. J. Kline, M. F. Toney, C. K. Chan, A. Agrawal, D. Gundlach, D. L. VanderHart, D. M. DeLongchamp. *Adv. Funct. Mater.* **2012**, *22*, 1255–1266. doi:10.1002/adfm.201102138.
- [24] E. W. Hansen, P. E. Kristiansen, B. Pedersen. *J. Phys. Chem. B* **1998**, *102*, 5444–5450. doi:10.1021/jp981753z.
- [25] D. L. VanderHart, C. R. Snyder. *Macromolecules* **2003**, *36*, 4813–4826. doi:10.1021/ma030131v.
- [26] A. Abragam, *The Principles of Nuclear Magnetism*, Oxford University Press, London, **1961**, pp. 97–132 264–353.
- [27] D. Torchia. *J. Magn. Reson.* **1978**, *30*, 613–616. doi:10.1016/0022-2364(78)90288-3.
- [28] S. Pankaj, M. J. Beiner. *J. Phys. Chem. B* **2010**, *114*, 15459–15465. doi:10.1021/jp1072999.
- [29] M. A. Ha, D. C. Apperley, B. W. Evans, I. M. Huxham, W. G. Jardine, R. J. Viator, D. Reis, B. Vian, M. C. Jarvis. *Plant J.* **1998**, *16*, 183–190. doi:10.1046/j.1365-313x.1998.00291.x.
- [30] M. Mehring, *Principles of High Resolution NMR in Solids*, Springer-Verlag, Berlin, **1983**, pp. 260–284.
- [31] G. C. Faria, E. R. de Azevedo, H. von Seggern. *Macromolecules* **2013**, *46*, 7865–7873. doi:10.1021/ma400648g.
- [32] R. F. Cossiglio, E. Kowalski, P. C. Rodrigues, L. Akcelrud, A. C. Bloise, E. R. de Azevedo, T. J. Bonagamba, T. D. Z. Atvars. *Macromolecules* **2005**, *38*, 925. doi:10.1021/ma048340i.
- [33] A. E. Bennett, C. M. Rienstra, M. Auger, K. V. Lakshmi, R. G. Griffin. *J. Chem. Phys.* **1995**, *103*, 6951. doi:10.1063/1.470372.
- [34] C. R. Morcombe, K. W. Zilm. *J. Magn. Reson.* **2003**, *162*, 479. doi:10.1016/S1090-7807(03)00082-X.
- [35] W. K. Rhim, D. D. Elleman, R. W. Vaughan. *J. Chem. Phys.* **1973**, *58*, 1772–1773. doi:10.1063/1.1679423.
- [36] A. Bielecki, D. J. Burum. *J. Magn. Reson. A* **1995**, *116*, 215–220. doi:10.1006/jmra.1995.0010.
- [37] A. L. Van Geet. *Anal. Chem.* **1968**, *40*, 2227–2229. doi:10.1021/ac50158a064.
- [38] A. L. Van Geet. *Anal. Chem.* **1970**, *42*, 679–680. doi:10.1021/ac60288a022.

## Supporting Information

Additional supporting information may be found in the online version of this article at the publisher's web site.